ADVANCED OPTICAL MATERIALS
www.advopticalmat.de

Altering the Reflection Phase for Nano-Polaritons: A Case Study of Hyperbolic Surface Polaritons in Hexagonal Boron Nitride

Mingyuan Chen, Stephen Sanders, Jialiang Shen, Jiahan Li, Eli Harris, Cheng-Chien Chen, Qiong Ma, James H. Edgar, Alejandro Manjavacas, and Siyuan Dai**

Polaritons—confined light–matter waves—in van der Waals (vdW) materials are a research frontier in light–matter interactions with demonstrated advances in nanophotonics. Reflection, as a fundamental phenomenon involving waves, is particularly important for vdW polaritons, predominantly because it enables the investigation of polariton standing waves using the scanning probe technique. While previous works demonstrate a rigid phase $\approx\pi/4$ for the polariton reflection, herein is reported the altering of the polariton reflection phase by varying the geometry of polaritonic microstructures for the case study of hyperbolic surface polaritons (HSPs) in hexagonal boron nitride (hBN). Specifically, it is demonstrated that the polariton reflection phase can be systematically altered by varying the corner angle of the hBN microstructures, and that it experiences a π jump around a specific angle. This behavior, which is a consequence of the mathematical nature of the reflection coefficient, is therefore expected in other physical phenomena.

1. Introduction

Polaritons[1] are hybrid electromagnetic modes resulting from the mixture of free-space photons and dipolar oscillations in materials. They possess a wavelength λ_p that is much smaller than that of free-space light λ_0, and their light–matter nature facilitates the control of their characteristics by varying the properties of the host materials. Polaritons, therefore, offer access to optical energy, wave properties, and light–matter interactions at subwavelength scales ($<\lambda_0$) that are promising for sensing, spectroscopy, biomedical treatments, and energy transfer applications.[1,2] The extraordinary properties of polaritons have recently been further developed in the context of van der Waals (vdW) materials,[3] where the reduced dimensionality leads to new virtues, such as atomic-scale localization,[4] dynamic tunability,[4a,b,5] topological protection,[6] and photonic hybrids.[5,7] Due to the ultrasmall lengthscale, polaritons in vdW materials are typically investigated using scanning probe optical microscopy[4b,5a,8] by directly imaging their standing waves. These standing waves are usually formed via reflection—the fundamental phenomenon of re-directing a wavefront within the same medium—of polaritons at crystal discontinuities, including edges,[4a,b,5a,8a–h] defects,[9] and steps.[10] Importantly, the reflection of polaritons exhibits a nontrivial phase ϕ (the complex reflection coefficient is $R = re^{i\phi}$, with r being the

M. Chen, J. Shen, S. Dai
Materials Research and Education Center
Department of Mechanical Engineering
Auburn University
Auburn, AL 36849, USA
E-mail: sdai@auburn.edu

S. Sanders, A. Manjavacas
Department of Physics and Astronomy
University of New Mexico
Albuquerque, NM 87106, USA
E-mail: a.manjavacas@csic.es

The ORCID identification number(s) for the author(s) of this article can be found under https://doi.org/10.1002/adom.202102723.

DOI: 10.1002/adom.202102723

J. Li, J. H. Edgar
Tim Taylor Department of Chemical Engineering
Kansas State University
Manhattan, KS 66506, USA

E. Harris, Q. Ma
Department of Physics
Boston College
Chestnut Hill, MA 02467, USA

C.-C. Chen
Department of Physics
University of Alabama at Birmingham
Birmingham, AL 35294, USA

A. Manjavacas
Instituto de Óptica (IO-CSIC)
Consejo Superior de Investigaciones Científicas
Madrid 28006, Spain

reflection amplitude) due to the Goos–Hänchen shift of polariton evanescent waves[11] at crystal discontinuities. As a result, right at the discontinuities, the interference is neither constructive nor destructive, but something in between. Despite extensive analysis of a variety of polaritonic vdW materials and heterostructures, the reflection phase ϕ remains at a universal value around $\pi/4$ without evident deviations.

In this work, we report the alteration of the polariton reflection phase in the case study of hyperbolic surface polaritons (HSPs) in hexagonal boron nitride (hBN). Specifically, we show that by varying the geometry of hBN microstructures, the reflection phase ϕ of HSPs can be modified and even reveals a π jump around a specific geometry. Accordingly, we demonstrate an evident position shift and switch from constructive to destructive interference of polariton standing waves. These experimental results are supported by rigorous numerical solutions of Maxwell's equations and are consistent with the mathematical properties of the reflection coefficient.

2. Results and Discussion

The phase of polariton reflection was investigated by imaging HSPs in hBN microstructures with a variety of geometries using scattering-type scanning near-field optical microscopy (s-SNOM, **Figure 1**). The imaging of polaritons using s-SNOM has been reported in a series of previous works.[4b,5a,8a–h,12] In the experiment (Figure 1a), an infrared (IR) laser illuminates the atomic force microscope (AFM) tip that acts as an antenna[13] to generate strong optical near-fields between the tip apex and sample. By bridging their momentum mismatch, these strong near-fields transfer energy from photons into polaritons and launch polariton waves in the hBN. As samples are scanned, the AFM tip also serves to detect the polariton standing wave oscillations. At a representative IR frequency ω = 1419 cm^{-1}, two types of phonon polaritons were imaged in the hBN microstructures (Figure 1a). These phonon polaritons are associated with the natural hyperbolic response of hBN with $\varepsilon_t\varepsilon_z < 0$[8a,14] ($\varepsilon_t$ and ε_z are the basal plane and vertical components of the permittivity tensor, respectively) inside the Reststrahlen bands (ω = 760–825 cm^{-1} and 1360–1614 cm^{-1}). Parallel to the edges, linear fringes were imaged with the strongest oscillation close to the edge, followed by weakly damped ones into the interior (Figure 1a,b). These fringes are standing wave oscillations of volume-confined hyperbolic phonon polaritons (HP^{2}s) propagating inside the hBN slab. Between the strongest fringe of the HP^{2}s and the hBN sidewall, a series of hot spots were imaged near the corner of the microstructure (Figure 1a–i). The hot spots exhibit a similar trend as that of the fringes of the HP^{2}s; namely, they display the strongest oscillation close to the corner, followed by damped ones away from it. These imaged oscillations are standing waves of HSPs confined along the hBN sidewalls[15] with a wavelength $\lambda_p \approx$ 80% of that of the HP^{2}s (Figure 1c).

As the corner angle α of the hBN microstructures varies, the HSP hot spots show a clear evolution. Specifically, the s-SNOM intensity $S(\omega)$ of the hot spots first decreases and then increases as α increases from 90° to 300° (Figure 1d–i). This evolution can be seen more clearly in the profiles taken from line cuts in the s-SNOM images (**Figure 2**a). Importantly, the position L (distance from the corner) of the HSP hot spots also evolves with α. In particular, the first peak of constructive interference shifts slightly toward the corner (L = 0) as α increases from 90° to 180° (see the red arrows in Figure 1d–f and the tilted black line in Figure 2a as a guide to the eye). The same occurs with the first dip due to destructive interference as α increases from 180° to 300°. Interestingly, the transition from $\alpha < 180°$ (blue curves) to $\alpha > 180°$ (red curves) results in a translation of the HSP hot spots, see the black arrow in Figure 2a as a guide to the eye. Note the s-SNOM data were obtained from

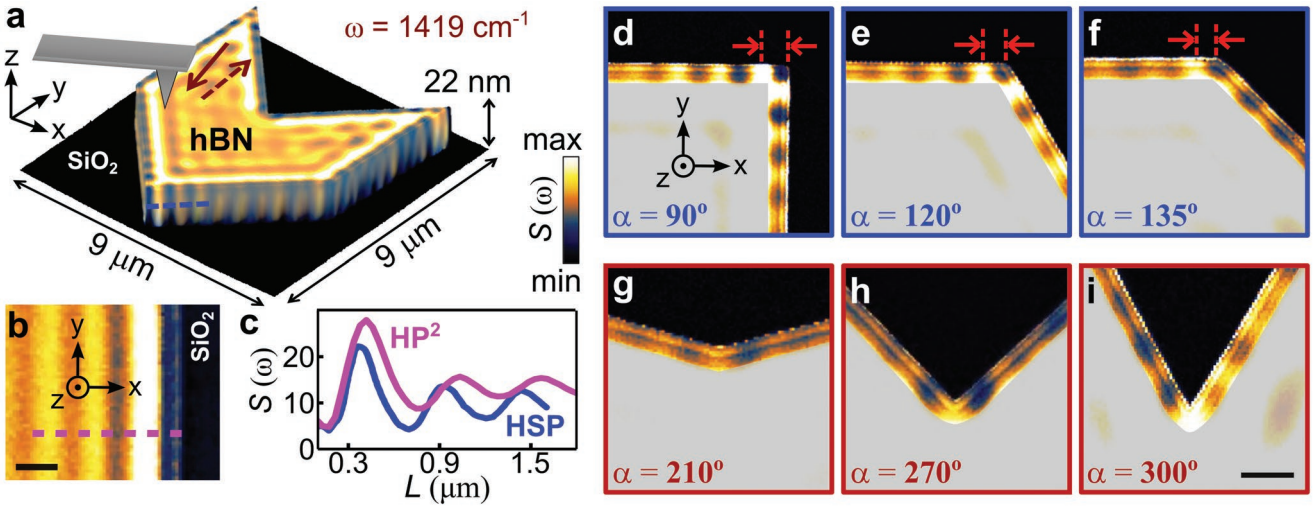

Figure 1. Scattering-type scanning near-field optical microscopy (s-SNOM) imaging of hyperbolic surface polaritons in hBN microstructures. a) Schematics of the s-SNOM experiment with a representative s-SNOM image on the hBN microstructure. b) s-SNOM image of volume-confined hyperbolic polaritons in hBN away from the edge of the microstructure. c) s-SNOM line profiles taken along the dashed lines in (a) and (b). d–i) s-SNOM image of hyperbolic surface polaritons in hBN for a corner angle α = 90°, 120°, 135°, 210°, 270°, and 300°. The IR frequency is 1419 cm^{-1}, and the thickness of the hBN crystal is 22 nm. Scale bar: 500 nm.

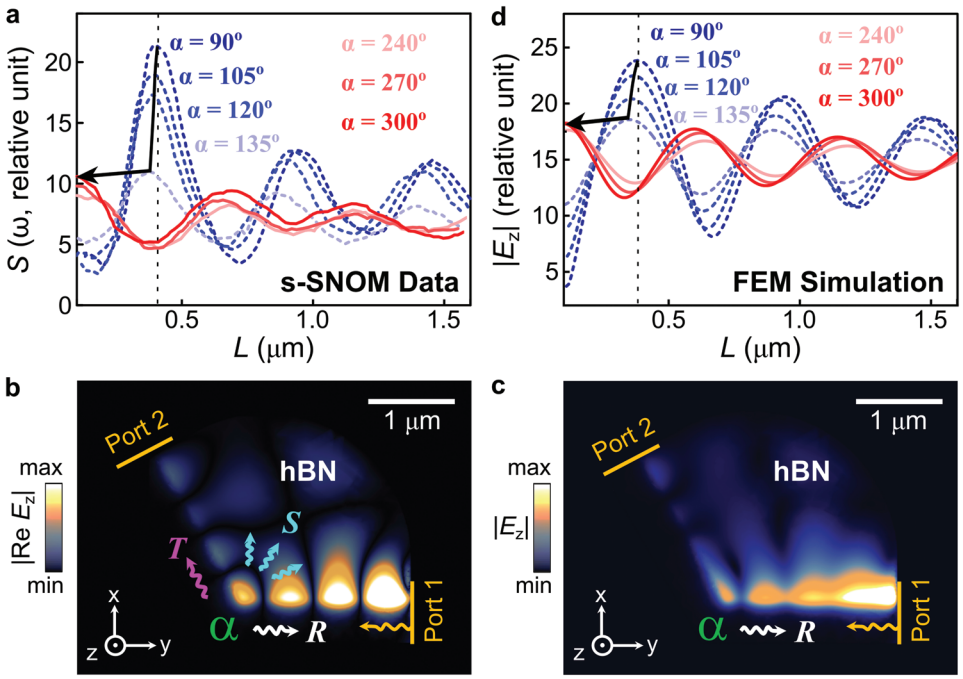

Figure 2. Altering the polariton reflection phase. a) s-SNOM line profiles taken from Figures 1d–i. Finite element method (FEM) simulation of HSPs in hBN microstructures showing either b) |Re E_z| or c) |E_z|. d) Normalized |E_z| line profiles along the edge of the microstructure.

microstructures etched from the same hBN slab. Therefore, all HSPs exhibit the same wavelength.

The change of intensity and position of the HSP hot spots reveals the evolution of the polariton reflection coefficient $R = re^{i\phi}$ with the corner angle α, since the imaged oscillations are standing waves arising from the interference between HSPs launched by the tip and their reflections from the corner. The intensities and positions of the HSP hot spots are associated with the reflection amplitude r and the phase ϕ, respectively. Following established procedures,[11c] we extracted r and ϕ from the s-SNOM data in **Figure 3**. The reflection amplitude r (Figure 3a) first decreases from 1 to 0, as the corner angle α is raised from 90° to 180°, then increases from 0 to 0.3 as α changes from 180° to 300°. On the other hand, the reflection phase ϕ has a three-step evolution with the corner angle α (Figure 3b). First, as α increases from 90° to 180°, ϕ slowly grows from ≈0.25π to ≈0.5π. Then, as α passes 180°, ϕ jumps from ≈0.5π to ≈–0.5π. Finally, as α further increases from 180° to 270°, ϕ again grows slightly. Therefore, the shift and translation of the HSP hot spots (Figures 1 and 2a) correspond to the evolution of the reflection phase ϕ with the corner angle α of hBN microstructures.

To support the experimental results, we modeled the HSPs of the hBN microstructures by rigorously solving Maxwell's equations using a finite element method (FEM) approach implemented in the commercial software COMSOL Multiphysics. Details of the FEM simulations are provided in Section S1 (Supporting Information). Briefly, we used two ports to launch and collect HSPs in the hBN microstructure (Figure 2b,c) and calculated the vertical component of the

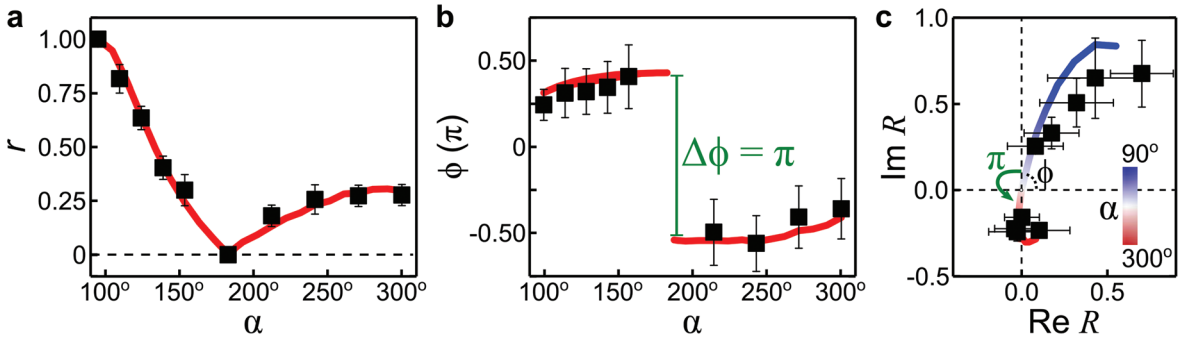

Figure 3. Evolution of the polariton reflection coefficient as a function of the corner angle α. a) Amplitude of the polariton reflection coefficient r. b) Phase of the polariton reflection coefficient ϕ. c) Evolution of the polariton reflection coefficient R in the complex plane. In all of the panels, the black squares show the experimental data, while the colored curves display the FEM simulation results.

electric field E_z at a distance 70 nm above it (Figure 2b,c). HSPs were launched from Port 1 and propagate along the sidewall toward the corner (angle α). Upon reaching the corner, the HSPs can be reflected (white arrow, Figure 2b), transmitted (pink arrow), and scattered (cyan arrow). The reflected HSPs propagate back toward Port 1 and interfere with the newly launched HSPs by the port, thus producing standing wave oscillations (Figure 2b,c). To better visualize the wave properties of the simulated HSPs, we extracted line profiles of $|E_z|$ along the edge of the structure, normalized them to the results for $\alpha = 180°$ (no oscillations, but only the baseline background is present), and plotted the resulting profiles in Figure 2d. These results agree well with our s-SNOM data (Figure 2a), showing a similar evolution with the corner angle α (see the black line and arrow as a guide to the eye). In order to extract the complex reflection $R = re^{i\phi}$ of the HSPs from our FEM simulation, we fitted the line profiles of Figure 2d to an analytical model resulting from the superposition of two plane waves describing the launched HSPs and their reflections from the corner.[5b,11c,16] Within this model, the electric field amplitude at a distance L from the corner is given by

$$\left|E_z(L)\right| = \left|E_0 e^{ik_p(L_0-L)} + E_0 r e^{i\phi} e^{ik_p L_0} e^{ik_p L}\right| \quad (1)$$

where E_0 is the initial amplitude of the electric field of the HSPs launched at Port 1, $k_p = 2\pi/\lambda_p$ is the momentum of the HSPs, and L_0 is the distance from Port 1 to the corner. The details of the fitting are provided in Section S2 (Supporting Information). The simulated reflection amplitude r and phase ϕ (Figure 3a,b, red curves) agree well with the s-SNOM data (Figure 3a,b, black squares).

Our results on the alteration of the polariton reflection phase and the corresponding standing waves can be related to a simple mathematic result: a differentiable parametric curve crossing the origin of the complex plane must undergo a π jump in its phase (Figure 3c). To explore this interpretation, we plot the reflection coefficient $R = re^{i\phi}$ in the complex plane, obtained from the experimental data (black squares) and FEM simulations (blue to red curve). For $90° < \alpha < 180°$ (blue curve and black squares in the first quadrant), the amplitude r decreases while the phase ϕ slowly increases as α grows. For $180° < \alpha < 300°$ (red curve and black squares in the third and fourth quadrant), both r and ϕ slightly increase (see Figure S5, Supporting Information for more angles). Importantly, when α crosses 180°, the reflection coefficient crosses the origin and its phase ϕ, as expected, undergoes a π jump (green arrow).

3. Conclusions

The combined s-SNOM experiments and electromagnetic simulations in Figures 1–3 reveal the alteration of the reflection phase of propagating HSPs in hBN. By varying the geometry of the hBN microstructures, the polariton reflection phase can be altered from the conventional value $\approx 0.25\pi$. It increases continuously to $\approx 0.5\pi$, and then jumps to $\approx -0.5\pi$. These results, which are a consequence of the mathematical properties of the reflection coefficient, are expected to occur in other polaritonic and physical phenomena. Another paradigmatic example is the Fresnel reflection coefficient of a dielectric interface; as the mismatch of the refractive indices of the two materials changes sign, the reflection coefficient undergoes a π phase shift. The ability to manipulate fundamental properties of polariton waves, as the reflection phase demonstrated here, by engineering the geometrical properties of the host materials can be further developed for applications in polaritonic circuits, transformation nano-light,[17] beaming,[18] biosensing,[19] and optical elements.[20] For instance, by using hBN microstructures with multiple corners and various corner angles, it is possible to create HSP cavity modes with fully controlled properties.

4. Experimental Section

Experimental Setup: Near-field nano-imaging: The IR nano-imaging of surface phonon polaritons in hBN was performed using a commercial scattering-type scanning near-field optical microscope (s-SNOM, www.neaspec.com) based on a tapping-mode AFM. In the experiments, an AFM tip (tip radius ≈ 10 nm) with a $PtIr_5$ coating was used. The AFM tip apex was illuminated by a monochromatic mid-IR quantum cascade laser (QCL) (www.daylightsolutions.com) with a frequency spanning from 850 to 1750 cm^{-1}. The s-SNOM nano-images were recorded by a pseudoheterodyne interferometric detection module with an AFM tapping frequency of 280 kHz and a tapping amplitude around 70 nm. The s-SNOM output signal was demodulated at the third harmonic of the tapping frequency to reduce the background signal.

Sample Synthesis: The natural abundant hBN crystals used in the experiments were grown at atmospheric pressure from molten metal solutions, as previously described.[21] Thin slabs were mechanically exfoliated from bulk hBN crystals and transferred onto a Si wafer covered with a 285 nm thick thermal silicon dioxide (SiO_2) film. Oxygen plasma etching was utilized to carve out the different geometrical patterns from the hBN slabs.

Supporting Information

Supporting Information is available from the Wiley Online Library or from the author.

Acknowledgements

M.C. and S.S. contributed equally to this work. Work at Auburn University was supported by National Science Foundation under Grant Nos. DMR-2005194 and OIA-2033454. S.D. and C.C. acknowledge the Seed funding from Alabama CPU2AL program, which is supported by National Science Foundation OIA-1655280. A.M. acknowledges Grant No. TEM-FLU PID2019-109502GA-I00 funded by MCIN/AEI/10.13039/501100011033 as well as the U.S. National Science Foundation (Grant No. DMR-1941680). hBN crystal growth was supported by National Science Foundation Grant CMMI-1538127 and Office of Naval Research award N00014-20-1-2474. J.S. acknowledges financial support from the Alabama Graduate Research Scholars Program (GRSP) funded through the Alabama Commission for Higher Education and administered by the Alabama EPSCoR. Q.M. acknowledges support from AFOSR grant FA9550-21-1-0319.

Conflict of Interest

The authors declare no conflict of interest.

Data Availability Statement

The data that support the findings of this study are available on request from the corresponding author. The data are not publicly available due to privacy or ethical restrictions.

Keywords

hexagonal boron nitride, phonon polaritons, reflection phase

Received: December 14, 2021
Revised: April 9, 2022
Published online: April 30, 2022

[1] a) J. A. Schuller, E. S. Barnard, W. Cai, Y. C. Jun, J. S. White, M. L. Brongersma, *Nat. Mater.* **2010**, *9*, 193; b) H. A. Atwater, *Sci. Am.* **2007**, *296*, 56.

[2] a) A. A. Govyadinov, A. Konecna, A. Chuvilin, S. Velez, I. Dolado, A. Y. Nikitin, S. Lopatin, F. Casanova, L. E. Hueso, J. Aizpurua, R. Hillenbrand, *Nat. Commun.* **2017**, *8*, 95; b) A. Konecna, J. Li, J. H. Edgar, F. J. G. de Abajo, J. A. Hachtel, *Small* **2021**, *17*, e2103404; c) N. Li, X. Guo, X. Yang, R. Qi, T. Qiao, Y. Li, R. Shi, Y. Li, K. Liu, Z. Xu, L. Liu, F. J. G. de Abajo, Q. Dai, E.-G. Wang, P. Gao, *Nat. Mater.* **2021**, *20*, 43.

[3] a) D. N. Basov, M. M. Fogler, F. J. G. de Abajo, *Science* **2016**, *354*, 1992; b) G. Hu, J. Shen, C.-W. Qiu, A. Alù, S. Dai, *Adv. Opt. Mater.* **2020**, *8*, 1901393; c) T. Low, A. Chaves, J. D. Caldwell, A. Kumar, N. X. Fang, P. Avouris, T. F. Heinz, F. Guinea, L. Martin-Moreno, F. Koppens, *Nat. Mater.* **2016**, *16*, 182.

[4] a) J. Chen, M. Badioli, P. Alonso-González, S. Thongrattanasiri, F. Huth, J. Osmond, M. Spasenović, A. Centeno, A. Pesquera, P. Godignon, A. Z. Elorza, N. Camara, F. J. G. de Abajo, R. Hillenbrand, F. H. L. Koppens, *Nature* **2012**, *487*, 77; b) Z. Fei, A. S. Rodin, G. O. Andreev, W. Bao, A. S. McLeod, M. Wagner, L. M. Zhang, Z. Zhao, M. Thiemens, G. Dominguez, M. M. Fogler, A. H. C. Neto, C. N. Lau, F. Keilmann, D. N. Basov, *Nature* **2012**, *487*, 82; c) D. A. Iranzo, S. Nanot, E. J. C. Dias, I. Epstein, C. Peng, D. K. Efetov, M. B. Lundeberg, R. Parret, J. Osmond, J.-Y. Hong, J. Kong, D. R. Englund, N. M. R. Peres, F. H. L. Koppens, *Science* **2018**, *360*, 291; d) S. Dai, W. Fang, N. Rivera, Y. Stehle, B.-Y. Jiang, J. Shen, R. Y. Tay, C. J. Ciccarino, Q. Ma, D. Rodan-Legrain, P. Jarillo-Herrero, E. H. T. Teo, M. M. Fogler, P. Narang, J. Kong, D. N. Basov, *Adv. Mater.* **2019**, *31*, 1806603.

[5] a) S. Dai, Q. Ma, M. K. Liu, T. Andersen, Z. Fei, M. D. Goldflam, M. Wagner, K. Watanabe, T. Taniguchi, M. Thiemens, F. Keilmann, G. C. A. M. Janssen, S. E. Zhu, P. Jarillo-Herrero, M. M. Fogler, D. N. Basov, *Nat. Nanotechnol.* **2015**, *10*, 682; b) A. Woessner, M. B. Lundeberg, Y. Gao, A. Principi, P. Alonso-González, M. Carrega, K. Watanabe, T. Taniguchi, G. Vignale, M. Polini, J. Hone, R. Hillenbrand, F. H. L. Koppens, *Nat. Mater.* **2015**, *14*, 421.

[6] a) T. P. Ginley, S. Law, *Adv. Opt. Mater.* **2018**, *6*, 1800113; b) J.-S. Wu, D. N. Basov, M. M. Fogler, *Phys. Rev. B* **2015**, *92*, 205430.

[7] a) J. D. Caldwell, I. Vurgaftman, J. G. Tischler, O. J. Glembocki, J. C. Owrutsky, T. L. Reinecke, *Nat. Nanotechnol.* **2016**, *11*, 9; b) T. G. Folland, A. Fali, S. T. White, J. R. Matson, S. Liu, N. A. Aghamiri, J. H. Edgar, R. F. Haglund, Y. Abate, J. D. Caldwell, *Nat. Commun.* **2018**, *9*, 4371.

[8] a) S. Dai, Z. Fei, Q. Ma, A. S. Rodin, M. Wagner, A. S. McLeod, M. K. Liu, W. Gannett, W. Regan, K. Watanabe, T. Taniguchi, M. Thiemens, G. Dominguez, A. H. C. Neto, A. Zettl, F. Keilmann, P. Jarillo-Herrero, M. M. Fogler, D. N. Basov, *Science* **2014**, *343*, 1125; b) M. Chen, X. Lin, T. H. Dinh, Z. Zheng, J. Shen, Q. Ma, H. Chen, P. Jarillo-Herrero, S. Dai, *Nat. Mater.* **2020**, *19*, 1307; c) W. Ma, P. Alonso-González, S. Li, A. Y. Nikitin, J. Yuan, J. Martín-Sánchez, J. Taboada-Gutiérrez, I. Amenabar, P. Li, S. Vélez, C. Tollan, Z. Dai, Y. Zhang, S. Sriram, K. Kalantar-Zadeh, S.-T. Lee, R. Hillenbrand, Q. Bao, *Nature* **2018**, *562*, 557; d) J. A. Gerber, S. Berweger, B. T. O'Callahan, M. B. Raschke, *Phys. Rev. Lett.* **2014**, *113*, 055502; e) L. V. Brown, M. Davanco, Z. Sun, A. Kretinin, Y. Chen, J. R. Matson, I. Vurgaftman, N. Sharac, A. J. Giles, M. M. Fogler, T. Taniguchi, K. Watanabe, K. S. Novoselov, S. A. Maier, A. Centrone, J. D. Caldwell, *Nano Lett.* **2018**, *18*, 1628; f) Z. Zheng, N. Xu, S. L. Oscurato, M. Tamagnone, F. Sun, Y. Jiang, Y. Ke, J. Chen, W. Huang, W. L. Wilson, A. Ambrosio, S. Deng, H. Chen, *Sci. Adv.* **2019**, *5*, 8690; g) P. Alonso-González, A. Y. Nikitin, F. Golmar, A. Centeno, A. Pesquera, S. Vélez, J. Chen, G. Navickaite, F. Koppens, A. Zurutuza, F. Casanova, L. E. Hueso, R. Hillenbrand, *Science* **2014**, *344*, 1369; h) X. G. Xu, B. G. Ghamsari, J.-H. Jiang, L. Gilburd, G. O. Andreev, C. Zhi, Y. Bando, D. Golberg, P. Berini, G. C. Walker, *Nat. Commun.* **2014**, *5*, 4782.

[9] a) Z. Fei, A. S. Rodin, W. Gannett, S. Dai, W. Regan, M. Wagner, M. K. Liu, A. S. McLeod, G. Dominguez, M. Thiemens, A. H. C. Neto, F. Keilmann, A. Zettl, R. Hillenbrand, M. M. Fogler, D. N. Basov, *Nat. Nanotechnol.* **2013**, *8*, 821; b) M. Schnell, P. S. Carney, R. Hillenbrand, *Nat. Commun.* **2014**, *5*, 3499.

[10] J. Chen, M. L. Nesterov, A. Y. Nikitin, S. Thongrattanasiri, P. Alonso-González, T. M. Slipchenko, F. Speck, M. Ostler, T. Seyller, I. Crassee, F. H. L. Koppens, L. Martin-Moreno, F. J. G. de Abajo, A. B. Kuzmenko, R. Hillenbrand, *Nano Lett.* **2013**, *13*, 6210.

[11] a) A. Y. Nikitin, T. Low, L. Martin-Moreno, *Phys. Rev. B* **2014**, *90*, 041407; b) X. Luo, C. Hu, B. Lyu, L. Yang, X. Zhou, A. Deng, J.-H. Kang, Z. Shi, *Phys. Rev. B* **2020**, *101*, 041407; c) J.-H. Kang, S. Wang, Z. Shi, W. Zhao, E. Yablonovitch, F. Wang, *Nano Lett.* **2017**, *17*, 1768.

[12] a) J. Chen, X. Lin, M. Chen, T. Low, H. Chen, S. Dai, *Appl. Phys. Lett.* **2021**, *119*, 240501; b) J. Shen, Z. Zheng, T. Dinh, C. Wang, M. Chen, P. Chen, Q. Ma, P. Jarillo-Herrero, L. Kang, S. Dai, *Appl. Phys. Lett.* **2022**, *120*, 113101.

[13] J. M. Atkin, S. Berweger, A. C. Jones, M. B. Raschke, *Adv. Phys.* **2012**, *61*, 745.

[14] a) J. D. Caldwell, A. V. Kretinin, Y. Chen, V. Giannini, M. M. Fogler, Y. Francescato, C. T. Ellis, J. G. Tischler, C. R. Woods, A. J. Giles, M. Hong, K. Watanabe, T. Taniguchi, S. A. Maier, K. S. Novoselov, *Nat. Commun.* **2014**, *5*, 5221; b) E. Yoxall, M. Schnell, A. Y. Nikitin, O. Txoperena, A. Woessner, M. B. Lundeberg, F. Casanova, L. E. Hueso, F. H. L. Koppens, R. Hillenbrand, *Nat. Photonics* **2015**, *9*, 674; c) Z. Shi, H. A. Bechtel, S. Berweger, Y. Sun, B. Zeng, C. Jin, H. Chang, M. C. Martin, M. B. Raschke, F. Wang, *ACS Photonics* **2015**, *2*, 790.

[15] a) S. Dai, M. Tymchenko, Y. Yang, Q. Ma, M. Pita-Vidal, K. Watanabe, T. Taniguchi, P. Jarillo-Herrero, M. M. Fogler, A. Alù, D. N. Basov, *Adv. Mater.* **2018**, *30*, 1706358; b) P. Li, I. Dolado, F. J. Alfaro-Mozaz, A. Y. Nikitin, F. Casanova, L. E. Hueso, S. Vélez, R. Hillenbrand, *Nano Lett.* **2017**, *17*, 228.

[16] S. Dai, Q. Ma, Y. Yang, J. Rosenfeld, M. D. Goldflam, A. McLeod, Z. Sun, T. I. Andersen, Z. Fei, M. Liu, Y. Shao, K. Watanabe, T. Taniguchi, M. Thiemens, F. Keilmann, P. Jarillo-Herrero, M. M. Fogler, D. N. Basov, *Nano Lett.* **2017**, *17*, 5285.

[17] A. Vakil, N. Engheta, *Science* **2011**, *332*, 1291.

[18] a) C. Sturm, D. Tanese, H. S. Nguyen, H. Flayac, E. Galopin, A. Lemaitre, I. Sagnes, D. Solnyshkov, A. Amo, G. Malpuech, J. Bloch, *Nat. Commun.* **2014**, *5*, 3278; b) Y. Wu, Q. Ou, S. Dong, G. Hu, G. Si, Z. Dai, C. W. Qiu, M. S. Fuhrer, S. Mokkapati, Q. Bao, *Adv. Mater.* **2021**, *33*, 2008070.

[19] a) S. H. Oh, H. Altug, X. Jin, T. Low, S. J. Koester, A. P. Ivanov, J. B. Edel, P. Avouris, M. S. Strano, *Nat. Commun.* **2021**, *12*, 3824; b) K. V. Sreekanth, S. Sreejith, S. Han, A. Mishra, X. Chen, H. Sun, C. T. Lim, R. Singh, *Nat. Commun.* **2018**, *9*, 369.

[20] S. A. Dereshgi, T. G. Folland, A. A. Murthy, X. Song, I. Tanriover, V. P. Dravid, J. D. Caldwell, K. Aydin, *Nat. Commun.* **2020**, *11*, 5771.

[21] J. Li, C. Yuan, C. Elias, J. Wang, X. Zhang, G. Ye, C. Huang, M. Kuball, G. Eda, J. M. Redwing, R. He, G. Cassabois, B. Gil, P. Valvin, T. Pelini, B. Liu, J. H. Edgar, *Chem. Mater.* **2020**, *32*, 5066.